2014 IEEE International Conference on Robotics & Automation (ICRA)
Hong Kong Convention and Exhibition Center
May 31 - June 7, 2014. Hong Kong, China

Development of High-Span Running Long Jumps for Humanoids

Patrick M. Wensing and David E. Orin

***Abstract*— This paper presents new methods to develop a running long jump for a simulated humanoid robot. Starting from a steady-state running motion, a new spring loaded inverted pendulum (SLIP) based 3D template model for a running jump is presented. The use of this model is motivated by a simpler model from biomechanics which describes the dynamics of human long jumpers in the sagittal plane. While previously only used to describe the thrust step of a long jump, this type of model is also shown to generate useful Center of Mass (CoM) trajectories to return to steady-state running upon landing. A principled optimization approach for this new template is described to generate reference CoM trajectories for maximum span which are able to be kinematically and dynamically retargeted to the humanoid. The key features of an optimal long jump are highlighted, and a task-space control approach to realize the motion on a humanoid is summarized. A video attachment to this paper shows an optimal long jump for a 6 m/s approach speed, where the humanoid is able to clear a large gap, and highlights the effects of non-optimal takeoff-velocity angles.**

I. Introduction

Despite the capability of biological systems to perform high-speed locomotion with ease, the ability to produce comparable behaviors in legged machines remains limited. In addition to the parallel challenges which face the systems' actuation, the control of high-speed locomotion is faced with difficulties due to legged systems' large state spaces and complex hybrid dynamics. In this paper we address the problem of generating a high-span running long jump for a high degree-of-freedom humanoid through trajectory optimization with a long jump template. With this approach, a running long jump is demonstrated in 3D dynamic simulation, shown in Fig. 1 and in the video attachment.

Although a challenge, the development of dynamic locomotion has the potential to provide humanoids with the ability to traverse more difficult terrain than is accessible through quasi-static locomotion alone. The problem of producing high-speed jumping has been studied previously through the use of genetic algorithms [1] or through graph-search-based methods combined with whole-body trajectory optimization [2]. Other whole-body trajectory optimization methods have restricted their search space through the use of motion capture [3] to simplify the problem.

Rather than focusing on the exact trajectory details of a dynamic motion, methods based on heuristics or template models attempt to identify and control the salient characteristics of a behavior. Hodgins et al. developed a series of hand-tuned controllers for many athletic motions [4] based on insight into the system's physics. The use of simple models of locomotion can be used to automate a large part of this process through developing template behaviors that are mapped to the humanoid through a lower-level controller. This methodology has been shown to enable walking [5] and high-speed running [6] in simulation with its extension studied here for a running long jump.

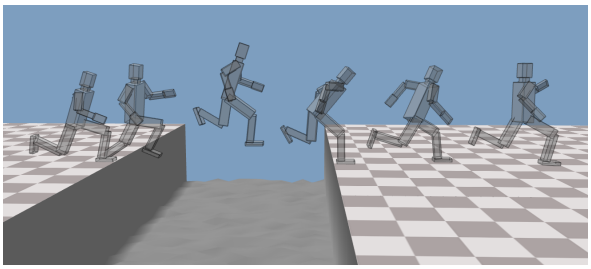

Fig. 1. A high-speed running long jump is demonstrated in 3D dynamic simulation by commanding the Center of Mass (CoM) dynamics of the humanoid to match those of an optimal SLIP-based long jump.

The remainder of this paper is organized as follows. Section II develops a 3D long jump template model which is based on a simpler planar model studied in biomechanics [7]. While the dynamics of takeoff and landing in a running jump share elements in common with high-speed running, the CoM dynamics experience a notable difference at the beginning of stance, as shown in Fig. 2. In this period, a large force peak contributes an initial vertical impulse to assist the production of maximum jump span. Section III presents a principled optimization-based approach to generate trajectories with a new 3D model that captures this effect. The results share many key characteristics with human long jump data. The whole-body humanoid control approach is summarized in Section IV which enables the performance of

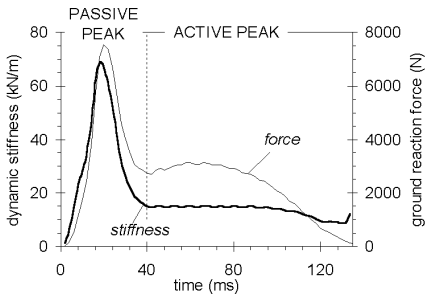

Fig. 2. Experimentally observed vertical ground reaction forces and leg stiffness for a human long jump, from [7]. The passive peak at the beginning is attributed to a forceful foot plant which decelerates the leg mass.

P. M. Wensing is a PhD student in the Department of Electrical and Computer Engineering, The Ohio State University: wensing.2@osu.edu
D. E. Orin is a Professor Emeritus in the Department of Electrical and Computer Engineering, The Ohio State University: orin.1@osu.edu

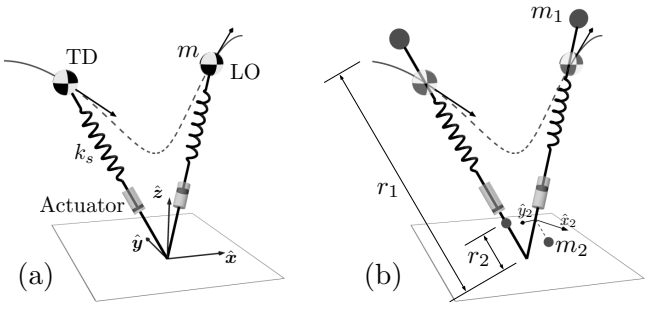

Fig. 3. (a) Leg extension 3D-SLIP (b) and long jump 3D-SLIP models to capture the salient requirements of producing a maximum-span running long jump. Following touchdown (TD) both models include a linear spring with stiffness k_s that is driven by a linear actuator. Ground contact terminates at liftoff (LO) when the spring reaches its rest length. The long jump 3D-SLIP model employs a main mass m_1 and small mass m_2 which together equal the total mass m. Mass 2 is attached to the spring leg at fixed radius r_2 via a nonlinear spring-damper. This mass is initialized along the leg at touchdown, but drifts off the leg throughout stance.

a running long jump in 3D dynamic simulation. Concluding remarks are provided in Section V.

II. Extended 3D-SLIP Template for Long Jump Optimization

While the standard 3D-SLIP model of locomotion can be used to describe the CoM dynamics of running with good fidelity, it lacks the capability to describe important characteristics of a running long jump. Biomechanics studies [7] have shown that human long jumpers employ a lengthened leg at takeoff in comparison to touchdown. In addition, human long jump data displays a passive ground reaction force (GRF) peak at the beginning of stance. Two modifications to the 3D-SLIP model are described below which provide the ability to capture these characteristics.

A. Leg Extension 3D-SLIP Model

In order to capture the leg lengthening effects found in human long jumping, active lengthening may be added to the 3D-SLIP model. Here, this lengthening is modeled through the incorporation of a linear actuator in series with the SLIP spring. This modification is shown in Fig. 3(a). The model consists of a point mass m and leg that experiences phases of stance and flight. The mass follows ballistic dynamics in flight wherein the massless leg is positioned for upcoming stance. Following touchdown (TD), a Hookean spring with constant k_s imparts forces onto the mass. The period of stance ends at liftoff (LO) when the spring once again reaches an unstretched length. Here, forward motion is assumed in the positive x-direction.

The dynamic evolution of the point mass is intended to describe the center of mass of a larger system. As such, its position in inertial coordinates is denoted as $\boldsymbol{p}_c \in \mathbb{R}^3$. The anchor point of the model is used to describe the foot position of a larger system, denoted here as $\boldsymbol{p}_f \in \mathbb{R}^3$. Letting $r = \|\boldsymbol{p}_c - \boldsymbol{p}_f\|$ and r_0 its value at TD, the spring imparts forces along the leg with magnitude:

$$f_s = k_s \left(r_0 + \ell_a - r\right) , \tag{1}$$

where ℓ_a is the length of the linear actuator, assumed to be zero at TD. This force provides the following stance dynamics for the mass:

$$\ddot{\boldsymbol{p}}_c = \frac{f_s}{m}\,\hat{\boldsymbol{r}} + \boldsymbol{g} \tag{2}$$

where $\hat{\boldsymbol{r}}$ is the unit vector along the SLIP leg and $\boldsymbol{g} = [0,\ 0,\ \text{-}9.81]^T$ is the gravity vector. Throughout this paper, a simple law is assumed for the actuator. Motivated by human data in the sagittal plane [7], its length is chosen proportional to the angular excursion of the SLIP leg projected onto the sagittal (x, z) plane. The angle of the SLIP leg from the vertical in the (x, z) plane is given by:

$$\theta_c = \text{atan2}\left(r\,\hat{\boldsymbol{x}}^T\hat{\boldsymbol{r}},\ r\,\hat{\boldsymbol{z}}^T\hat{\boldsymbol{r}}\right), \tag{3}$$

with $\theta_{c,0}$ defined to be its value at touchdown. From this definition, the actuator length is assumed here to take the form

$$\ell_a = b_a\left(\theta_c - \theta_{c,0}\right) \tag{4}$$

where b_a is a positive constant of proportionality to be tuned through optimization in Section III. Forward running jumps are dominated by motion in the positive x-direction, and thus θ_c and ℓ_a are monotonically increasing.

B. Long Jump 3D-SLIP Model

In addition to active lengthening, human long jumpers plant their stance foot more forcefully prior to takeoff, resulting in a large force peak that decelerates the stance leg mass. This force peak injects additional vertical impulse, which is a key requirement of jumping for distance. The foot plant behavior can be introduced through the addition of a second mass to the Leg Extension SLIP model, shown in Fig. 3(b). In this model, the mass m_2 represents the stance leg mass, and is connected to the SLIP leg at a fixed distance r_2 through a nonlinear spring-damper. The large mass m_1 is positioned at radius r_1 and is still driven by the SLIP spring. Similar to before, the spring produces forces

$$f_s = k_s\left(r_{1,0} + \ell_a - r_1\right) \tag{5}$$

directed along $\hat{\boldsymbol{r}}$. These forces act only on m_1. To describe the position of mass m_2, coordinate vectors $\hat{\boldsymbol{x}}_2$ and $\hat{\boldsymbol{y}}_2$ are attached to and rotate with the SLIP leg. Combined with $\hat{\boldsymbol{r}}$ these provide a coordinate system with rotation matrix:

$$\boldsymbol{R} = \begin{bmatrix}\hat{\boldsymbol{x}}_2 & \hat{\boldsymbol{y}}_2 & \hat{\boldsymbol{r}}\end{bmatrix}. \tag{6}$$

Letting $\boldsymbol{p}_2'$ be the position of mass m_2 relative to this frame, its position in inertial coordinates is given as:

$$\boldsymbol{p}_2 = r_2\,\hat{\boldsymbol{r}} + \boldsymbol{R}\,\boldsymbol{p}_2'. \tag{7}$$

Again motivated by the planar case, a nonlinear spring-damper force is applied to mass m_2 in order to return it to position $r_2\hat{\boldsymbol{r}}$ in inertial coordinates. Here, we assume a locally coordinate-decoupled force given by:

$$\boldsymbol{f}_2 = \boldsymbol{R}\begin{bmatrix}-(k_2\,p_{2,x}' + d_2\,\dot{p}_{2,x}')\cdot\left|p_{2,x}'\right|^{c_2}\\ -(k_2\,p_{2,y}' + d_2\,\dot{p}_{2,y}')\cdot\left|p_{2,y}'\right|^{c_2}\\ -(k_2\,p_{2,z}' + d_2\,\dot{p}_{2,z}')\cdot\left|p_{2,z}'\right|^{c_2}\end{bmatrix}, \tag{8}$$

r_2	k_2	d_2	c_2	m_1	m_2
0.25 m	14.6 kN/m	$10^{8.5}$ N·s / m	2.8	58.1 kg	14.5 kg

TABLE I

FIXED PARAMETER VALUES FOR LONG JUMP 3D-SLIP DYNAMICS.

where k_2, d_2 and c_2 are constants. The inclusion of nonlinear effects is justified by considering the dynamics that the additional mass is intended to capture; when planted forcefully, the foot experiences ground contact forces which can be described well with nonlinear contact models [8]. Fixed selections for c_2, d_2, r_2, and k_2 are given in Table I. The value of r_2 in this table is chosen to be approximately one quarter of the extended virtual leg length (0.975 m) of the humanoid considered in Section IV. Masses m_1 and m_2 represent 80% and 20% of the mass of the humanoid. Spring-damper constants for a planar long jump model running at 8.2 m/s [7] were tuned to produce values for k_2, d_2, and c_2 which resulted in similar passive force peaks for speeds in the range of 4 m/s to 6 m/s with this model. While fixed here, further adaptation of these parameters could provide benefits to jump span. In the following section, an optimization-based approach will be presented to select the rest of the parameters for the Long Jump 3D-SLIP model.

During stance, simulation of the Long Jump SLIP model in 3D introduces additional complexities due to the forces on the second mass. Turning first to kinematics, the position of this system can be specified uniquely by r_1, $\boldsymbol{p}_2'$, and $\boldsymbol{R}$ (which includes $\hat{\boldsymbol{r}}$). The system velocity is then given by $\dot{r}_1$, $\dot{\boldsymbol{p}}_2'$, and $\boldsymbol{\omega}$. Here $\boldsymbol{\omega}$ gives the angular velocity of $\boldsymbol{R}$ in inertial coordinates. $\boldsymbol{R}$ is stored using a quaternion to avoid singularities and may be integrated with quaternion rates given in [9]. Due to its nonlinear effects, the force $\boldsymbol{f}_2$ may in fact create moments around the SLIP leg that must be countered by constraint moments at the anchor point. Yet, in order for the anchor point to represent a center of pressure (CoP), these constraint moments must only exist in the $\hat{\boldsymbol{z}}$ direction. To handle this requirement, the anchor point is treated as a soft point contact [10]. This type of contact is able to produce moments normal to the plane. Under this assumption, the angular velocity can be chosen to take the form $\boldsymbol{\omega} = [\omega_x, \omega_y, 0]^T$. It can be shown that restricting angular velocities to this form imposes a nonholonomic constraint on the achievable rotations $\boldsymbol{R}$. Thus, this constraint precludes the use of any 2 element parameterization for the rotation matrix $\boldsymbol{R}$ such as 2 Euler angles. The full stance dynamics are summarized in Table II. Note that the equation for $[\dot{\omega}_x, \dot{\omega}_y]^T$ arises from equating the net moment on the SLIP leg (about $\boldsymbol{p}_f$) to its rate of change in angular momentum about $\boldsymbol{p}_f$. The equations for $\ddot{r}_1$ and $\ddot{\boldsymbol{p}}_2'$ can be derived through a second differentiation of the kinematic equations and use of Newton's second law.

III. LONG JUMP OPTIMIZATION

Given an initial state of the CoM, this section will provide an optimization-based method to produce a reference CoM trajectory for a maximum-span long jump. As shown in Fig. 4, the span s of a long jump is considered from footprint to footprint, across the thrust and landing steps. The total span is comprised of three components, two on the ground and a main component in flight. The following subsections will present a staged optimization process which first generates a thrust step, and then subsequently generates a landing step.

Kinematics

$$\boldsymbol{p}_1 = r_1\,\hat{\boldsymbol{r}} \qquad \dot{\boldsymbol{p}}_1 = \dot{r}_1\,\hat{\boldsymbol{r}} + \boldsymbol{\omega}\times\boldsymbol{p}_1$$
$$\boldsymbol{p}_2 = r_2\,\hat{\boldsymbol{r}} + \boldsymbol{R}\boldsymbol{p}_2' \qquad \dot{\boldsymbol{p}}_2 = \boldsymbol{\omega}\times\boldsymbol{p}_2 + \boldsymbol{R}\dot{\boldsymbol{p}}_2'$$

Dynamics

$$\boldsymbol{\beta} := m_1\,\boldsymbol{p}_1\times\boldsymbol{g} - \boldsymbol{p}_2\times\boldsymbol{f}_2 - m_1\,\boldsymbol{p}_1\times(2\,\dot{r}_1\,\boldsymbol{\omega}\times\hat{\boldsymbol{r}} + \boldsymbol{\omega}\times\boldsymbol{\omega}\times\boldsymbol{p}_1)$$
$$\boldsymbol{I} := m_1\,\boldsymbol{S}(\boldsymbol{p}_1)\,\boldsymbol{S}(\boldsymbol{p}_1)^T$$
$$\begin{bmatrix}\dot{\omega}_x\\ \dot{\omega}_y\end{bmatrix} = \begin{bmatrix}I_{xx} & I_{xy}\\ I_{yx} & I_{yy}\end{bmatrix}^{-1}\begin{bmatrix}\beta_x\\ \beta_y\end{bmatrix}$$
$$\ddot{r}_1 = \tfrac{f_s}{m_1} + \hat{\boldsymbol{r}}^T\boldsymbol{g} - \hat{\boldsymbol{r}}^T(\boldsymbol{\omega}\times\boldsymbol{\omega}\times\boldsymbol{p}_1)$$
$$\ddot{\boldsymbol{p}}_2' = \boldsymbol{R}^T\left(\tfrac{\boldsymbol{f}_2}{m_2} + \boldsymbol{g}\right) - \boldsymbol{R}^T(\dot{\boldsymbol{\omega}}\times\boldsymbol{p}_2 + \boldsymbol{\omega}\times\boldsymbol{\omega}\times\boldsymbol{p}_2 + 2\,\boldsymbol{\omega}\times\boldsymbol{R}\dot{\boldsymbol{p}}_2')$$

Note: $\boldsymbol{S}(\boldsymbol{p}) \in \mathbb{R}^{3\times3}$ is a skew symmetric cross product matrix providing $\boldsymbol{S}(\boldsymbol{p})\,\boldsymbol{p}_b = \boldsymbol{p}\times\boldsymbol{p}_b$ for every $\boldsymbol{p}_b \in \mathbb{R}^3$.

TABLE II

EQUATIONS OF MOTION FOR THE LONG JUMP 3D-SLIP MODEL.

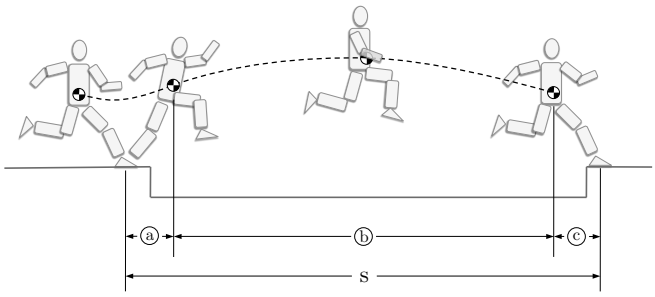

Fig. 4. The span s of the long jump is broken into three components: a) the takeoff span, measured from the center of the stance foot to the horizontal position of the CoM at liftoff, b) the flight span, measured from the CoM at liftoff to the CoM at the subsequent touchdown, and c) the touchdown span, again measured from CoM to the center of the foot.

A. Thrust Step Optimization

Starting from a steady-state run, the thrust step of the long jump serves to generate a large vertical CoM velocity before takeoff. Generation of this vertical velocity requires proper selection of the leg's touchdown configuration as well as proper coordination of the leg's stroke during stance. These details are first coordinated on the Long Jump 3D-SLIP model before being mapped to the humanoid as described in Section IV. The touchdown span (ⓒ in Fig. 4) does not vary greatly across long jumps, and thus was considered fixed when optimizing the thrust step.

The optimization approach used here applies constrained nonlinear optimization methods, where dynamic simulation of the Long Jump 3D-SLIP is applied to evaluate the objective (jump span) and constraints. The optimization variables and constraints are summarized in Table III with further detail provided below. Simulation of the Long Jump 3D-SLIP model is carried out starting at the top-of-flight (TOF) before thrust, continuing through stance, and ending at the subsequent TD. Assuming an approach speed of v_x in the forward direction, the TOF CoM State is given from our previous methods [6]. For a fixed approach speed the optimization problem is given in general form as:

$$\max_{\mathbf{x}} \; s(\mathbf{x}) \tag{9}$$

$$\text{s.t. } \underline{\mathbf{g}} \leq \mathbf{g}(\mathbf{x}) \leq \overline{\mathbf{g}} \tag{10}$$

$$\underline{\mathbf{x}} \leq \mathbf{x} \leq \overline{\mathbf{x}} \tag{11}$$

where $\mathbf{x} = [\theta,\, \phi,\, \ell_{TD},\, k_s,\, b_a]^T$ is the vector of optimization variables, $s(\mathbf{x})$ provides the simulated span, and $\mathbf{g}(\mathbf{x}) \in \mathbb{R}^4$ contains simulated results for the constrained quantities in Table III. The markings $\underline{\cdot}$ and $\overline{\cdot}$ represent upper and lower bounds. Leg touchdown angles θ and ϕ, and a touchdown leg length ℓ_{TD} specify the SLIP foot position in flight:

$$\boldsymbol{p}_f = \boldsymbol{p}_c + \boldsymbol{p}_{hip} + \ell_{TD} \begin{bmatrix} \sin(\theta)\cos(\phi) \\ -\sin(\theta)\sin(\phi) \\ -\cos(\theta) \end{bmatrix} \tag{12}$$

where $\boldsymbol{p}_{hip}$ approximates the vector between the CoM and the hip of the next stance leg [6]. Roughly, θ controls the forward angle of the leg and ϕ controls the foot's lateral placement. Given selections for θ, ϕ, and ℓ_{TD}, the state of the CoM at TD can be computed from ballistic physics without simulation. At TD, the CoM state is then mapped to a state of the Long Jump 3D-SLIP with mass m_2 along the leg[1].

During stance, the behavior of the Long Jump 3D-SLIP model is influenced by its leg stiffness k_s, and its actuator lengthening b_a. Improper selection of k_s or b_a often results in trajectories that are not transferable to the humanoid. For instance, selection of a small spring stiffness may result in a soft landing with too low of a CoM height, while a high spring stiffness may result in GRFs that are infeasible to be generated by the humanoid. Similarly, a high leg lengthening constant b_a may result in a CoM position that is beyond the kinematic limits of the humanoid. A limit on $\|\boldsymbol{p}_c - \boldsymbol{p}_f\|$ at LO is set to approximate this constraint. As a final constraint, the lateral velocity at LO is constrained to be zero, in order to prevent lateral motion in flight.

Following stance, ballistic motion is assumed for the CoM and allows for the flight span (ⓑ in Fig. 4) to be computed. A fixed touchdown CoM height, taken from steady-state running, is considered across all simulations. MATLAB's `fmincon` with its active-set algorithm was used to solve (9)-(11) and generate the maximum-span reference motion.

[1]The assumption that mass m_2 is along the leg in flight allows only two parameters θ, ϕ to describe the orientation of the leg. At touchdown, the leg orientation is converted to quaternions for simulation of the stance leg orientation dynamics which evolve on $SO(3)$.

	Lower Bnd.	Upper Bnd.
Variables		
Touchdown Angle, θ	0	$\frac{\pi}{4}$
Touchdown Angle, ϕ	$-\frac{\pi}{4}$	$\frac{\pi}{4}$
Touchdown Length, ℓ_{TD}	0.7 m	0.97 m
Spring Stiffness, k_s	10 kN/m	100 kN/m
Lengthening Parameter, b_a	-2 m/rad	2 m/rad
Constraints		
Maximum Vertical GRF	-	4 kN
Minimum CoM Height	0.72 m	-
$\|\boldsymbol{p}_c - \boldsymbol{p}_f\|$ at LO	-	1.0 m
CoM Lateral Velocity at LO	0 m/s	0 m/s

TABLE III
THRUST STEP OPTIMIZATION SUMMARY

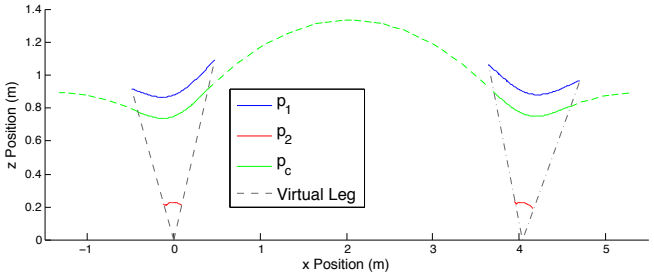

Fig. 5. Simple model trajectories in the sagittal plane for an optimized long jump following a 6 m/s run. Dashed trajectories for $\boldsymbol{p}_c$ indicate flight. The model begins with a steady-state run, experiences an explosive thrust step, and then employs a single recovery step to return to periodic motion.

B. Landing Step Optimization

The landing step optimization develops a trajectory of the Long Jump 3D-SLIP model that starts in flight, following the optimized thrust step, and returns to steady-state running at the subsequent TOF. Once complete, a continuous reference CoM trajectory is available, starting from and ending at the CoM motion for running as shown in Fig. 5.

The optimization process to generate a landing step largely mirrors that of the thrust step, with the main exception being its objective. Simulation occurs from the TOF following thrust, continues through the landing step, and terminates at the subsequent TOF. Landing optimization employs the same variables and bounds in Table III. The constraint on $\|\boldsymbol{p}_c - \boldsymbol{p}_f\|$ is replaced with a lower bound of 0.85 m to prevent an excessively shortened leg at TD. The lateral LO velocity is unconstrained, and all other constraints remain the same. Rather than maximizing span, the landing step optimization minimizes the squared error between the achieved CoM TOF state following landing and that of steady-state running. Again, MATLAB's `fmincon` was used to optimize the SLIP touchdown and stroke parameters. With this approach, optimized trajectories for landing were able to perfectly match the TOF CoM state for steady-state running. Optimized variables $\mathbf{x}$ for the thrust and land steps are shown in Table IV, and result in a 4.12 m long jump.

C. Optimization Results

The long jump trajectories produced through this process exhibit characteristics common to human long jumpers. The

Step	θ	ϕ	ℓ_{TD}	k_s	b_a
Thrust	28.8°	−12.3°	0.89 m	16.5 kN/m	0.16 m/rad
Landing	24.8°	−14.4°	0.97 m	14.4 kN/m	−0.01 m/rad

TABLE IV

OPTIMIZED LONG JUMP 3D-SLIP PARAMETERS FOR A 6 M/S APPROACH

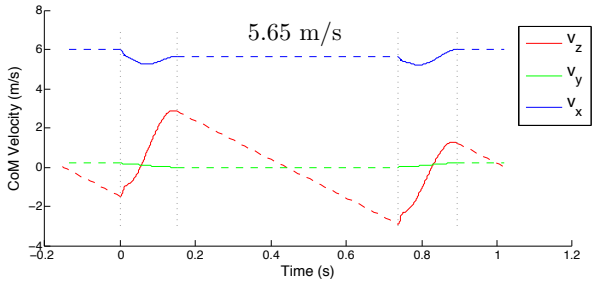

Fig. 6. CoM Velocity for an optimized long jump following a 6 m/s run. During the thrust period before the long jump, the system loses forward velocity (v_x) through a pole-vault action over its stance leg that generates vertical velocity (v_z). Dashed segments indicate periods of ballistic flight.

CoM velocity for an optimized long jump with a 6 m/s approach speed is shown in Fig. 6. As noted on the figure, the thrust step results in a net loss in forward velocity. This slight decrease in forward velocity from $0-170$ ms is accompanied by a large increase in vertical velocity. This exchange of velocity components has been conceptualized as a "pivot" [11] in the biomechanics literature and is inherent to the SLIP-based model used here. At higher speeds, human long jumpers may lose over 1.0 m/s in forward velocity in order to achieve additional span [12].

All of the constraints placed on the Long Jump 3D-SLIP model are limiting to its performance, and provide insight into the key characteristics of jumping for distance. Figure 7 shows trajectories of the CoM Height, approximate virtual leg length $\|\boldsymbol{p}_c - \boldsymbol{p}_f\|$, and vertical GRFs for the optimum. Constraints on each of these quantities are active. Given the constraint on the vertical GRF, vertical impulse may only be increased through additional time in stance. For the optimum, a maximum time in stance is achieved by coordinating stiffness and lengthening of the leg to utilize the full allowable range of its stroke. A sensitivity analysis of the optimum reveals the importance of this principle, as the optimum span increases by 9.7 cm per 1 cm of additional length, and by 4.8 cm per 1 cm of additional allowable vertical excursion downward.

Aside from proper leg coordination for maximum stroke, it is important to select proper touchdown angles to maximize the benefit of the "pivoting" or pole-vaulting effect over the stance leg. To understand this effect, the long jump optimization was repeated with an additional constraint placed on the angle of the CoM velocity at takeoff relative to the horizontal. As shown in Fig. 8, this takeoff-velocity angle γ_{LO} negatively affects span when too high or too low. Low takeoff angles are obtained by landing with the foot largely underneath the body, minimizing any vaulting effect. High takeoff angles are obtained by landing with the foot further

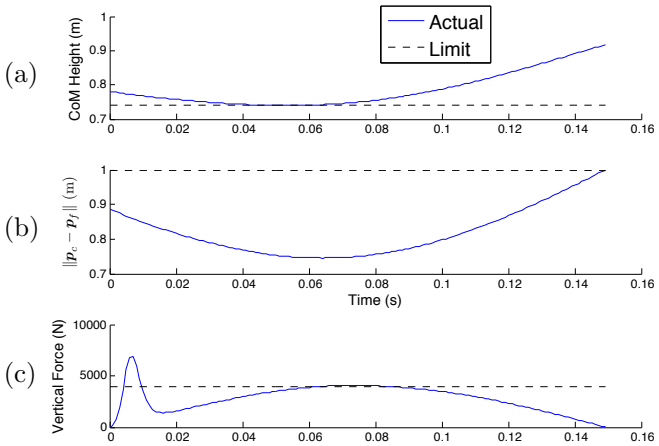

Fig. 7. Active constraints on the optimum long jump. The optimum extends its time on the ground by (a) traveling as low as allowed to allow for maximum stroke and (b) coordinating its leg thrust to achieve maximum leg extension at takeoff. (c) The optimum also applies the maximum allowable vertical GRF to impart the largest vertical impulse.

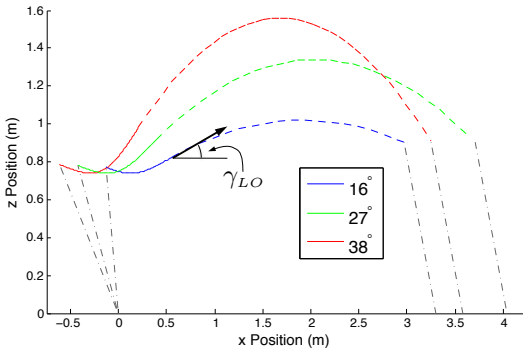

Fig. 8. Effect of takeoff-velocity angle γ_{LO} on jump span. At takeoff angles below the optimum, insufficient vertical velocity is created in stance. At takeoff angles higher than the optimum, horizontal velocity is sacrificed for vertical velocity without benefit to span.

in front at TD, but can lose too much forward velocity.

To illustrate this tradeoff further, takeoff-velocity magnitude is plotted against takeoff-velocity angle in Fig. 9. Approximating the flight as having equal takeoff and landing heights, the flight span for each takeoff state can be computed as $\frac{2}{g}v_x v_y$. The contours on Fig. 9 represent takeoff states that result in the same estimated flight span. Despite this simplification, the graphical optimum for the estimated flight span is within a degree of the optimum for total span. Note that the maximum attainable takeoff-velocity diminishes with increased takeoff-velocity angle. This effect is not present in the traditional ballistic shooting problem, where the takeoff-velocity magnitude is fixed and the optimum takeoff-velocity angle is $45°$. Due to the diminishing takeoff-velocity effect for the long jump, the optimum takeoff-velocity angle is much lower. While the importance of takeoff angle has been shown for human long jumping [13], the optimization constraints imposed here enable similar properties to emerge from our model. Notice that at lower speeds, the optimal takeoff-velocity angle shifts to higher values, as additional vertical velocity may be generated with

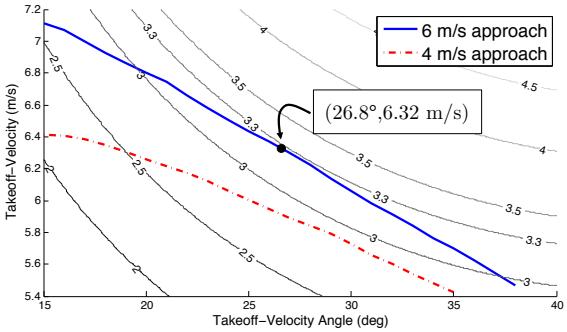

Fig. 9. Maximal takeoff-velocity versus takeoff-velocity angle for a 6 m/s and 4 m/s running approach. Contours indicate magnitude and angle combinations which produce equivalent estimated flight spans $\frac{2}{g}v_x v_y$. The point with optimal total span for a 6 m/s approach is shown and corresponds to a near optimum of estimated flight span.

less detriment to forward speed. This trend agrees with human studies [14].

IV. Humanoid Running Long Jump

Performance of the running long jump by the humanoid can be accomplished with an extension to the state-machine-based task-space control approach applied in humanoid running [6]. This previous work allowed for the humanoid to run at high speeds through tracking of hand-tuned foot trajectories and an optimized CoM reference. The reference CoM motions developed here fit within this framework without difficulty and allow for the previous task-space approach for running to be applied. As in this previous work, the task-space controller is able to handle omissions in the template, such as contact impulses or the effects of rotational inertia, through application of centroidal momentum control.

A video attachment to the paper shows the humanoid tracking an optimal long jump following a 6 m/s run. The video can also be found on the web at:

`http://go.osu.edu/Wensing_Orin_ICRA2014`

The humanoid used in the simulation applies torque control at its joints in order to realize the reference CoM motion. While space permits only a high-level description of the control approach, the reader is referred to [6], [15] for further details. At each control step, an embedding of the template Long Jump 3D-SLIP CoM dynamics is accomplished through real-time optimization of joint torques as well as GRFs below the feet in stance [15]. An angular momentum controller is applied in stance to regulate the angular momentum at takeoff and prevent excess body rotation in flight. While arm motion targets are supplied to match the swing of the opposite leg, the low task weights given to these joints allows the momentum controller to adjust the upper body motions to maintain balance.

V. Conclusions

This paper has presented new methods to develop a running long jump for humanoid robots. The new Long Jump 3D-SLIP model has shown to produce optimal CoM trajectories with properties that are consistent with human long jumpers. With the constraints imposed on the model, the takeoff-velocity angle has been shown to be a key characteristic for achieving a maximum jump distance. The constrained nonlinear optimization formulation discussed allows for optimal leg coordination and takeoff-velocity angle to be produced automatically for any given CoM approach state. This strategy allows a previous controller for high-speed running to be applied to control both the thrust and landing steps. The capability of this methodology to generate balanced yet aggressive dynamic motions encourages further study to investigate agile behaviors such as high-speed turning or to create additional acrobatic behaviors in flight. Further, investigation of real-time optimization approaches for these systems has the potential to enable intelligent, reactive behaviors to respond to additional uncertainties in the environment and model.

VI. Acknowledgments

This work was supported by a National Science Foundation Graduate Research Fellowship to Patrick Wensing, and by Grant No. CNS-0960061 from the NSF with a subaward to The Ohio State University.

References

[1] D. Krasny and D. Orin, "Evolution of dynamic maneuvers in a 3D galloping quadruped robot," in *IEEE Int. Conf. on Robotics and Automation*, pp. 1084–1089, 2006.

[2] C. Dellin and S. Srinivasa, "A framework for extreme locomotion planning," in *IEEE Int. Conf. on Robotics and Automation*, pp. 989–996, May 2012.

[3] A. Safonova, J. K. Hodgins, and N. S. Pollard, "Synthesizing physically realistic human motion in low-dimensional, behavior-specific spaces," in *Proc. of ACM SIGGRAPH*, vol. 23, (New York, NY, USA), pp. 514–521, August 2004.

[4] J. K. Hodgins, W. L. Wooten, D. C. Brogan, and J. F. O'Brien, "Animating human athletics," in *Proc. of ACM SIGGRAPH*, (New York, NY, USA), pp. 71–78, 1995.

[5] I. Mordatch, M. de Lasa, and A. Hertzmann, "Robust physics-based locomotion using low-dimensional planning," in *Proc. of ACM SIGGRAPH*, vol. 29, (New York, NY, USA), pp. 71:1–71:8, July 2010.

[6] P. M. Wensing and D. E. Orin, "High-speed humanoid running through control with a 3D-SLIP model," in *Proc. of the IEEE/RSJ Int. Conf. on Intelligent Rob. and Sys.*, pp. 5134–5140, Nov. 2013.

[7] A. Seyfarth, A. Friedrichs, V. Wank, and R. Blickhan, "Dynamics of the long jump," *J. of Biomech.*, vol. 32, no. 12, pp. 1259–1267, 1999.

[8] D. Marhefka and D. Orin, "A compliant contact model with nonlinear damping for simulation of robotic systems," *IEEE Trans. on Sys., Man and Cybernetics*, vol. 29, no. 6, pp. 566–572, 1999.

[9] K. Waldron and J. Schmiedeler, "Chapter 1: Kinematics," in *Springer Handbook of Robotics* (B. Siciliano and O. Khatib, eds.), New York: Springer, 2008.

[10] J. Kerr and B. Roth, "Analysis of multifingered hands," *The International Journal of Robotics Research*, vol. 4, no. 4, pp. 3–17, 1986.

[11] P. Graham-Smith and A. Lees, "A three-dimensional kinematic analysis of the long jump take-off.," *Journal of Sports Sciences*, vol. 23, no. 9, pp. 891–903, 2005.

[12] J. G. Hay, J. A. Miller, and R. W. Canterna, "The techniques of elite male long jumpers," *Journal of Biomechanics*, vol. 19, no. 10, pp. 855–866, 1986.

[13] N. P. Linthorne, M. S. Guzman, and L. A. Bridgett, "Optimum take-off angle in the long jump," *Journal of Sports Sciences*, vol. 23, no. 7, pp. 703–712, 2005.

[14] L. A. Bridgett and N. P. Linthorne, "Changes in long jump take-off technique with increasing run-up speed," *Journal of Sports Sciences*, vol. 24, pp. 889–897, Aug. 2006.

[15] P. M. Wensing and D. E. Orin, "Generation of dynamic humanoid behaviors through task-space control with conic optimization," in *IEEE Int. Conf. on Rob. and Automation*, pp. 3088–3094, May 2013.